NANOWIRE-NANOPARTICLE CONJUGATE PHOTOLYTIC DEVICES FOR RENEWABLE HYDROGEN PRODUCTION

By

SEAN KELLY MACLASKEY

Bachelor of Science in Aerospace Engineering

Oklahoma State University

Stillwater, Oklahoma

2009

Submitted to the Faculty of the
Graduate College of
Oklahoma State University
in partial fulfillment of
the requirements for
the Degree of
MASTER OF SCIENCE
July, 2011

NANOWIRE-NANOPARTICLE CONJUGATE

PHOTOLYTIC DEVICES FOR RENEWABLE

HYDROGEN PRODUCTION

Thesis Approved:

Dr. A. Kaan Kalkan

Thesis Advisor

Dr. Kevin Ausman

Dr. David Rubenstein

Dr. Mark E. Payton

Dean of the Graduate College

ACKNOWLEDGMENTS

I would like to thank the members of my defense committee, Dr. Kevin Ausman and Dr. David Rubenstein. Thank you very much to Dr. Hongbing Lu for introducing me to research as an undergraduate in engineering, and sparking my interest into this field. A special thank you goes to my advisor, Dr. Kalkan, for giving me the opportunity to work on this exciting project and for advising me in my academics and research.

Thank you to my research colleagues in the NML for their encouragement and input into my research. Thank you to Karthikeyan Ramachandriya Dharman, Robert Ingraham, and Dr. Mark Wilkins for their assistance with GC. Thank you to Özge Topal, Ryan Jones, and Mr. Terry Colberg for help with SEM and TEM. Also, thank you to Rama Krishna Ede for the invaluable suggestions and support.

Finally, thank you to Brooke, for your patience and love, I could not have done it without your support every step of the way. Thank you to my friends and family, with a special thank you to my parents, for their unending guidance throughout my entire college career and my life. The example you have set for me to follow and your loving support are what have made my accomplishments and achievements possible.

TABLE OF CONTENTS

Chapter Page

LIST OF TABLES

Table Page

LIST OF FIGURES

Figure Page

CHAPTER 1

INTRODUCTION

By the year 2035, energy consumption across the globe is reported to increase by as much as 50% [1]. While it is still uncertain the exact amount of obtainable oil that remains in world petroleum reserves, estimates of reserve volumes and current estimates of oil consumption track the end of fossil fuels to possibly come within the next 50 years. The development of a clean, renewable alternative to fossil fuels for the world's energy needs has proven to be a remarkable challenge for researchers and scientists over the past four decades. Beginning in the 1970's with oil and gas shortages, and reoccurring with the recent swells in oil prices in 2008 and 2011, research into a viable option has become a flourishing field of scientific interest. As new technologies arise and past methods are made more efficient, the solution to the world's energy problems may be found in the smallest molecule known to man. While other options have emerged over the years, very few can compete with the potential of hydrogen (H_2) in terms of energy density and clean emissions. When comparing specific energy, H_2 is shown to be over three times the magnitude of gasoline or diesel fuel [2]. In terms of emissions, H_2 is a clean-burning fuel that is considered to have zero-emission. When it is burned with oxygen (O_2), essentially its only emission is water (H_2O). When these advantages are combined with the use of a renewable energy source, such as solar energy, for producing the H_2 and O_2, and a completely renewable, clean-burning energy alternative is delivered.

Hydrogen can be produced by a variety of means, but one of the most economical and environmentally friendly ways is by splitting water into H_2 and O_2. Water is abundant and inexpensive, covering 70% of the earth's surface, so it is an ideal source of H_2. The energy required for the decomposition of water is 1.23 eV. If this energy is harvested from the Sun, the largest energy reservoir known, then the "holy grail" of renewable fuel production can be achieved. However, water does not absorb 1.23 eV photons or higher energy photons up to 6.5 eV (190 nm). Hence, photodissociation of water does not occur if water is exposed with photon energies below 6.5 eV. In 1972, Honda and Fujishima resolved this problem by first absorbing the photons in a photocatalyst and then using the photogenerated electrons and holes to drive the reduction and oxidation reactions to break water to hydrogen and oxygen, respectively.

The oxidation reaction in this approach is given by:

$$H_2O + 2h\nu\ (sunlight) \ \rightarrow \ 2e^- + 2H^+ + \frac{1}{2}O_2 \tag{1.1}$$

Reduction of H^+ is given by:

$$2H^+ + 2e^- \ \rightarrow \ H_2 \tag{1.2}$$

The objective of this thesis is to develop a nanowire-nanoparticle (NW-NP) conjugate photolytic device producing H_2. By using this novel concept, the goal is to increase the efficiency of photolysis at low cost. Using materials at the nanoscale, solar energy can be more efficiently harvested and converted. The primary advantage of the present approach is to decrease the distances that photoelectrons and photoholes have to travel before they are channeled to reduction and oxidation reactions, respectively. Thereby, the energy imparted from photons is not wasted to heat by electron-hole recombination. In the present work, the novel technique of using vanadium oxyhydrate ($V_3O_7{\cdot}H_2O$) NWs decorated with gold (Au) NPs for photolytic H_2 production is explored in detail.

Research interest concerning photolytic water splitting has been intermittent since the early findings of Honda and Fujishima in 1972 [3]. Since then, a number of designs have been

presented, yet none of these have discovered an efficient and sustainable option for fuel production from solar energy. This 40-year struggle with no success may be attributed to a number of factors. First, photooxidation of electrode materials can inhibit production in a short time of exposure, a very common issue with most of the earlier attempts in photolysis. Also, inefficient channeling of electrons to the redox reaction can give much lower efficiencies, as useful energy is lost in the form of electron-hole recombination. Lastly, the insufficient absorption of light is another cause for low efficiency.

What this project provides is an efficient means of conducting photolysis for H_2 fuel production, using nanodevices comprised of transition metal-oxide NWs decorated with metal NPs. In previous attempts at sustained photolysis of water, electrical stimulus was required to sustain the production of H_2 and O_2. This thesis demonstrates the proof of concept of a new photolytic device, which exhibits Quantum Efficiency (QE) of 19.28% under 470 nm (2.64 eV) radiation. This value is a considerable achievement when comparing it with the limited number of previous designs using the visible light spectrum, which will be discussed in the next chapter of the present thesis. The Internal Conversion Efficiency (ICE) of this device was found to be 8.98%. In addition to demonstrating H_2 bubbling at 470 nm, this photolytic concept has displayed gas production at alternative light wavelengths such as 405, 425, 525, and 605 nm (3.06, 2.92, 2.36, and 2.05 eV, respectively) covering a significant range of the visible spectrum. Previously, visible light photolysis was demonstrated only at the near-UV regime.

The present thesis delivers a completely different perspective on photolytic hydrogen production from past attempts. Using the novel concept of NP-NW conjugates, photolytic nanodevices are virtually created via self-assembly upon solution chemistry. In terms of raw materials required and operation of a photolytic array, the costs would be equal to PV cells currently in the market. However, the method used to build this type of photolytic device is relatively simple, saving time and money on production costs. In addition, startup capital is

minimized in comparison to the cost of building and maintaining the advanced cleanroom facilities required for fabricating silicon-based PV cells.

The material used in this experiment, the vanadium oxyhydrate ($V_3O_7{\cdot}H_2O$) aerogel, is a recently discovered material and has been shown to absorb light efficiently [4]. $V_3O_7{\cdot}H_2O$ nanowires are synthesized by sol-gel chemistry to form a wet aerogel. Next, they are dried in liquid carbon dioxide (CO_2), and subsequently suspended in deionized (DI) water. The sol-gel process is simple in comparison to standard PV device manufacturing, with no specialized facility requirements and expensive equipment and labor costs. In addition, Au NPs decorating the surface of $V_3O_7{\cdot}H_2O$ NWs (cathode) are synthesized by a simple chemical reduction technique in solution. Nanoparticles also enhance optical by plasmonic effects.

The organization of the proceeding chapters will be presented in the following order. In the next chapter, a discussion of the background of photolysis will be presented. In addition, a review of recent attempts at producing a sustainable method of producing H_2 via photolysis will be given. Experimental procedures utilized during the present thesis will be explained in Chapter 3. Further, the experimental results will be provided and discussed, in Chapter 4. Finally, the ultimate conclusions drawn from the present investigation will be presented.

CHAPTER 2

BACKGROUND

2.1 Photolysis of Water

Hydrogen (H_2) production via photolysis (cleaving of water by light energy) is a technique, by which renewable H_2 fuel can be produced from a sustainable energy source such as sunlight. A detailed review of photolysis is presented below.

2.1.1 Optical Properties of Water

In Nature, water does not inherently dissociate into the elements H_2 and O_2 under light irradiation. The natural and abundant presence of water on earth is proof of this fact; otherwise water would be nonexistent due to constant radiation from the Sun. Water only absorbs a small amount of the visible light spectrum, which helps to explain its transparency; as without light absorption, a material is perceived to have no color. The energy required for light absorption by water is far into the UV region, at energies above 6.5 eV [3,5]. Since water does not absorb visible light naturally, electronic transitions by photon excitation are impossible without a light-absorbing photocatalyst. Photocatalysis is a method by which water can be exposed to lower photon energies, but still can be cleaved by driving the redox reactions required for photolysis. Using this principle, the photo-electrode absorbs photon energy to create the electron-hole pair for oxidation

and reduction of the surrounding H_2O and H_2, respectively. With the discovery of more efficient light- absorbing photoanodes, lower photon energies in the visible spectrum can be used for water splitting, while earlier methods were only possible through the use of UV light.

2.1.2 Working Principle of Photolysis

H_2 and O_2 can be produced from the photodissociation of water by the reduction of H^+ and oxidation of H_2O. For photolytic water splitting, the energy from a photon, hν, is used to create electron-hole pairs (e^- and h^+ respectively) as shown by the reaction

$$2h\nu \rightarrow 2e^- + 2h^+ \tag{2.1}$$

The photogenerated holes (h^+) created from the above activity are used in the oxidation reaction of water as denoted by

$$2h^+ + H_2O \rightarrow {}^1\!/_2\, O_2 + 2H^+ \tag{2.2}$$

The photogenerated electrons (e^-) are used for reduction of H^+. This reaction takes place at the cathode and is shown in the equation below.

$$2e^- + 2H^+ \rightarrow H_2 \tag{2.3}$$

Finally, the overall oxidation/reduction or redox reaction can be illustrated by

$$2h\nu + H_2O \rightarrow {}^1\!/_2\, O_2 + H_2 \tag{2.4}$$

In Figure 2.1 below, a typical photolytic device is shown. In this figure, an electron-hole pair is generated by the absorption of a photon in the photoanode material. Subsequently, the photo-generated electron travels to the cathode, where the reduction reaction takes place for H^+/H_2. At the photoanode, the remaining photohole induces the splitting of water into H^+ and O_2. This simple concept has been the fundamental design for most subsequent studies in photolysis of

water since its conception in 1972. While subsequent designs have been capable of sustained water cleavage by light, the possibility for recombination of electron-hole pairs is high for this concept, due to the extended distances required for travel from the location of photon absorption to the redox reactions (i.e., inside the photoanode).

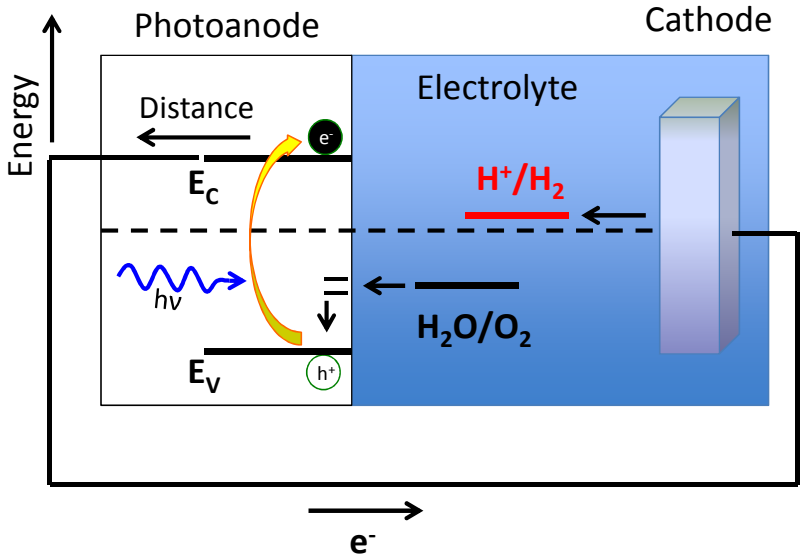

Figure 2.1: Photogenerated electron/hole pair and the subsequent channeling to redox reactions.

2.2 Development of Photolytic Devices

The first study into photolytic water splitting was published in 1972. In this work, Honda and Fujishima were able to cleave H_2 and O_2 from a molecule of H_2O using a semiconducting n-type titanium dioxide (TiO_2) photoanode with a Platinum (Pt) cathode and UV light [3]. This work required a bias voltage to sustain the reaction. The quantum efficiency (QE) of this concept was estimated at 0.1 (10%). A diagram showing this concept can be viewed in Figure 2.2.

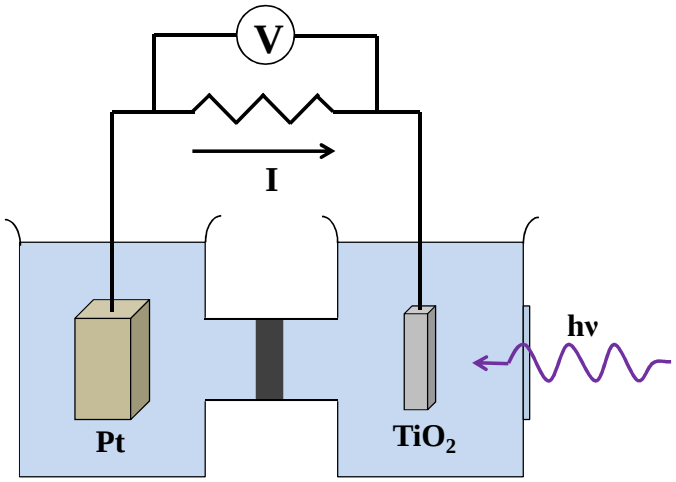

Figure 2.2: Photolytic device designed by Honda and Fujishima in 1972 [3].

In the years following the first discovery of photolytic water splitting, over 130 designs have been developed using a wide range of materials [6]. However, of these new designs, the large majority has only made slight variations to the initial concept displayed in Figure 2.2. A study conducted by Kawai *et al.* in 1979 attempted to bubble H_2 using a mixture of powdered TiO_2, RuO_2, and active carbon on a glass substrate, and while the reaction was favorable, hydrogen evolution was not sustainable past a few hours [7]. In 1981, Borgarello *et al.* demonstrated a photolytic concept utilizing TiO_2 as the photoanode, but was doped with ultrafine deposits of Pt and RuO_2 [8]. The introduction of these catalyst materials proved to increase the system's efficiency in coupling to the oxidation/reduction reactions. This particular design demonstrated production values of 2-3 mL/hr of H_2, yet the overall efficiency did not surpass that of Honda's work. Recently, in a study conducted by Varghese *et al.*, water was split using micron-length nanotubes made from the same titanium oxide material used previously, producing a maximum efficiency of 12.25% under UV light [9]. This work showed long-term stability and a resistance to photodegradation over months of use. Still, the greatest hurdle to visible light photolysis going forward has been the discovery of a material with sufficient absorption of visible light, or the shifting of a current material's absorption modes to absorb these lower energy

wavelengths of light. In a paper authored by Mallouk in 2010, it was noted that still the majority of photolytic concepts only were capable of using the edge of the blue light spectrum, and that very few were able to operate using the visible light spectrum [11].

A *Nature* article authored by Grätzel in 2001 discussed the capability of a modern photolytic cell to replace the photovoltaic cell as the dominant technology of solar energy production in the near future [12]. Since the first discovery of photolytic water splitting, the perceived upper-limit for QE of visible-light irradiated devices has been 10% [13]. Currently, the most efficient means of cleaving water by photolysis utilizes the photon energy of UV light ($\lambda <$ 400 nm) and the standard TiO_2 photoanode. From a broader standpoint of efficiencies, since wavelengths contained in this range only comprise 4% of the electromagnetic energy provided by the sun, the conversion efficiency of a UV-illuminated system would be diminished considerably in comparison to visible-light devices [10]. In Table 2.1, past attempts in photolytic water splitting are listed with their major findings. The trend over the past 40 years has shown a slow progression of devices operating at the visible range, but still showed a limited QE (or quantum yield QY) for these visible light-operated concepts. The common design for the presented designs below is the use of bulk-scale electrode materials, with little deviation from the original model demonstrated by Honda and Fujishima. The introduction of sensitizers used as catalysts for photolysis has been fundamental to the increase of efficiencies, but never before has a concept been demonstrated using nanowire-nanoparticle (NW-NP) conjugates. In addition, the development of visible-light driven devices has been especially slow, since lower incident photon energies provided by higher wavelengths of light provide extremely low conversion efficiencies for the traditional concept. For photolytic hydrogen production to be feasible going forward, the ability to absorb and convert visible light energy is paramount. The novel design presented in this thesis aims to convert visible light into useable hydrogen fuel by utilizing this NW-NP conjugate device concept.

Table 2.1: Previous investigations into photolysis and their findings [3,6,8,10,14,16-17]

Inventor	Year	Material	Result	Light	Comments
Fujishima/Honda [3]	1972	TiO_2, Pt	QE 10%	UV	500 W source External bias
Grätzel/Borgarello [8]	1981	TiO_2, Pt, RuO_2	3mL H_2/hr	UV	450 W source 25mL solution
Domen/Sayama [6]	1996	Ni-$Rb_4Ta_6O_{17}$, Ni-$Rb_4Nb_6O_{17}$	QE 5-10%	330 nm	400 W source 1 g to 350 mL H_2O
Arakawa/Zou [10]	2001	$In_{1-x}Ni_xTaO_4$	QY 0.66%	402/420 nm	300 W source 0.5 g to 250 mL H_2O
Kato/Kudo [16]	2003	$NaTO_3$, NiO	QY 56%	270 nm	400 W Hg source 1 g to 390 mL reactant solution
Domen/Maeda [17]	2006	$(Ga_{1-x}Zn_x)(N_{1-x}O_x)$	QE 2.5%	420-440 nm	Hg Lamp Powder in H_2O
Belcher/Nam [14]	2010	M13 Virus, ZnDPEG	.114mL O_2/hr	550 nm	No H_2

2.3 Major Challenges in Photolysis

2.3.1 Electrode Requirements

The lack of advancement in photolytic device efficiencies can be attributed to many factors; however the strict requirements placed on electrode materials make photolysis such a challenging area of study. This includes four main factors, correct energy band structure, minimizing overpotential, maximizing light absorption, and elimination of photodegradation. These requirements are detailed below.

1. The valence and conduction band levels must be positioned in a manner that promotes the proper oxidation and reduction reactions for splitting water. The energy level of the conduction band must be equal or higher than the electropotential of the reduction reaction, and the valence band must be equal or lower than the electropotential of the

oxidation reaction. Without these conditions, the reaction will have a much lower tendency without the addition of an external voltage source.

2. The electrodes must be stable, specifically the photoanode. The hole generated in the photoanode can alternatively oxidize the anode material if the anode is capable of undergoing an oxidation reaction with water. It is possible to obtain stable photoanodes with transition metal oxides (TMOs). TMOs are strongly stabilized by oxygen, in particular if the transition metal is at its highest oxidation state. Hence, there are no oxidation pathways in H_2O. On the other hand, TMOs can also be strong absorbers of visible light due to transitions between bonding states (valence band) to nonbonding d-states (conduction band).
3. The chosen photoanode must absorb solar radiation efficiently. The efficient absorption of solar energy increases external conversion efficiency (CE).
4. A proper electrode must minimize the overpotential, also known as electrochemical polarization. A poor material selection can present issues with duration of exposure and lowered output. This effect can be caused by the formation of a thin oxidation layer, a monolayer of O_2, or a monolayer of H_2 on the surface of the anode or cathode, reducing the reduction and oxidation potentials. The polarization of a photolytic device can also lead to secondary corrosion reactions including the photodegradation process discussed in requirement 2.

2.3.2 Proposed Electrode Material

The vanadium oxyhydrate ($V_3O_7{\cdot}H_2O$) aerogel is a TMO hydrate created by the sol-gel process. The sol-gel preparation consists of the solution chemistry of a precursor material, most commonly a metal oxide. Critical drying is performed in liquid CO_2 after sol-gel synthesis, to prevent structural collapse due to surface tension forces at the nanoscale. This material is known to be built on a “bird’s nest” structure of NWs. The nanoeffect on the selected electrode material

is believed to increase QE from conventional methods by reducing the probability of recombination of photogenerated electron-hole pairs. Since the distances these electron hole pairs have to travel for redox reactions is much shorter than with conventional electrodes, losses attributed to recombination are reduced. Because this material has only recently been discovered, many electronic and optical properties have yet to be investigated. The present thesis conducts further investigation into the electronic and optical properties of the $V_3O_7{\cdot}H_2O$ aerogel and its nanostructure.

The novel approach this thesis presents for photolytic water splitting uses NW-NP conjugates rather than the standard photo-anode/cathode system. The incorporated Au NPs on the surface of the photoanode is theorized to serve as the cathode for H^+ reduction. The use of silver (Ag) NPs was recently employed with TiO_2 nanorods, showing an enhancement of the photocatalytic process due to the "charge-separation" effect [18]. This effect is believed to increase the lifetime of photogenerated electron-hole pairs, reducing the potential for immediate recombination, and the losses attributed to it [19]. Plasmonic metal NPs, such as Au and Ag, can also increase optical absorption efficiency by near-field enhancements. In literature, the deposition of metal NPs (i.e., Au, Ag, Pt) on semiconductor surfaces has shown orders of magnitude increase in Raman scattering [20]. This effect may translate to enhancement of optical absorption, which would lead to an increase in CE. Another advantage with the use of NPs is the possibility of charge-induced voltage, elevating the energy of the NP until the appropriate energy is achieved for the reduction reaction to take place. This effect is due to the small capacitance of NPs. However, this effect is only advantageous for band energy lower than the electropotential required in the reduction of H^+. Figure 2.3 shows the photolytic concept implemented in this thesis.

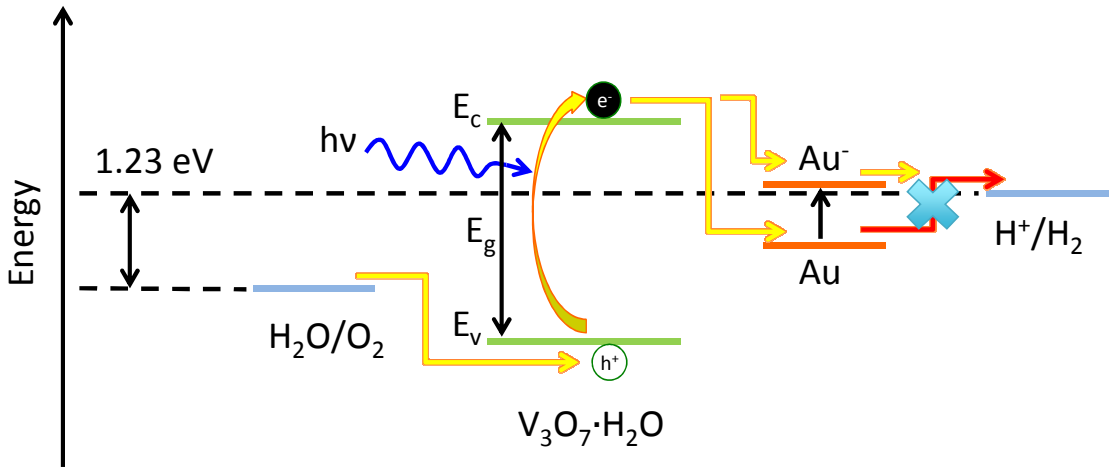

Figure 2.3: Photolytic device concept developed in the present thesis (energy levels not to scale)

CHAPTER 3

METHODOLOGY

3.1 Fabrication

3.1.1 Sol-Gel Synthesis of $V_3O_7{\cdot}H_2O$ Aerogels

Vanadium oxyhydrate ($V_3O_7{\cdot}H_2O$) aerogels are synthesized via sol-gel chemistry, and then supercritically dried in liquid carbon dioxide (CO_2) to prevent collapse of the inherent "bird's nest" nanowire structure. For wet-gel synthesis of $V_3O_7{\cdot}H_2O$, 5.8 mL of deionized (DI) water is mixed with 11.34 mL of acetone, then subsequently added to 2.4 mL of vanadium (V) tripropoxide, $VO(OCH_2CH_2CH_3)_3$. To prevent immediate gelation upon mixture, the two separate solutions were cooled in a dry ice/acetone bath (-78 °C) until ice appeared in the water/acetone mixture, and viscosity increased in the vanadium (V) tripropoxide solution. Before mixing of the two solutions, the water/acetone mixture was shaken vigorously until the ice fragments were no longer present. Then, the water/acetone mixture was added to vanadium (V) tripropoxide rapidly. Immediately, the obtained mixture was shaken for 10-15 s and subsequently transferred to polyethylene syringes (Becton Dickinson & Co., Luer-Lok™ Tip, 5 mL), and sealed with Parafilm. These wet gels were aged for 5 days in the syringes. After aging, the gels were removed from syringes and placed in containers filled with anhydrous acetone. To aid in flushing of the impurities and to remove any excess water from the material, the acetone was changed every 24

hours for four days. Subsequently, the gels were dried via supercritical drying in CO_2 to fully remove the exchanged acetone.

After the acetone flush, the aerogel is supercritically dried using the E3000 critical point dryer (CPD) apparatus (Quorum Technologies, West Sussex, UK). The drying chamber is filled with acetone prior to the wet gel's insertion into the CPD, to prevent the natural drying process. By pumping cold water around the exterior of the apparatus, the dryer is cooled to a temperature below 20 °C to prevent the incoming compressed CO_2 from freezing immediately. Once the system is pre-cooled, high-pressure CO_2 is introduced into the chamber, and the pressure is held constant at 55 bar (800 psi). After 20 minutes, the CO_2/acetone mixture is flushed from the chamber, and CO_2 is once again introduced to the system to the same conditions as before. This process is repeated 8-10 times, to ensure the CO_2 has fully penetrated the sample, and all residual acetone is flushed from the aerogel. Following the completion of the flushing steps, the chamber is heated and pressurized above the critical point of CO_2 of 31.1 °C and 73.9 bar (1071 psi). By the same method used to pre-cool the system, warm water is pumped through the system constantly to maintain a constant 40 °C and 83 bar (1200 psi). Upon reaching its supercritical state, the pressure and temperature are held constant for 2 hours. Once the sample has been dried in the supercritical fluid for 2 hours, the vent valve is opened partially, allowing for a slow, steady pressure release over a period of 3-4 hours. The final aerogel is observed to be a dull green, fragile solid of extremely low density. Multiple $V_3O_7{\cdot}H_2O$ aerogels can be seen after the critical drying process in Figure 3.1.

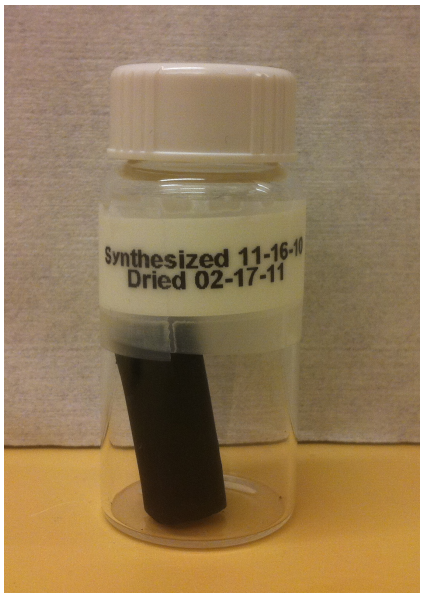

Figure 3.1: Dry $V_3O_7 \cdot H_2O$ aerogel sample after supercritical drying

3.1.2 Fabrication of Photolytic Nanodevices

Upon synthesis and critical drying, $V_3O_7 \cdot H_2O$ NWs are dissolved in DI water at a concentration of 3.4 g/L and stored as a stock solution before characterization by UV-visible spectroscopy, electron microscopy, and photolytic device fabrication. The photolytic nanodevice suspension is shown in an optical cell in Figure 3.2. Device fabrication involves simply reduction of Au nanoparticles (NPs). For this process, 0.1 mL of $HAuCl_4$ (0.1 M) is diluted in 2 mL of DI water, after which 2 mL of 3.4 g/L $V_3O_7 \cdot H_2O$ is added. The mixture is then shaken vigorously. A completed NW-NP conjugate device consists of 0.0025 M $HAuCl_4$, and 1.7 g/L of $V_3O_7 \cdot H_2O$ NWs.

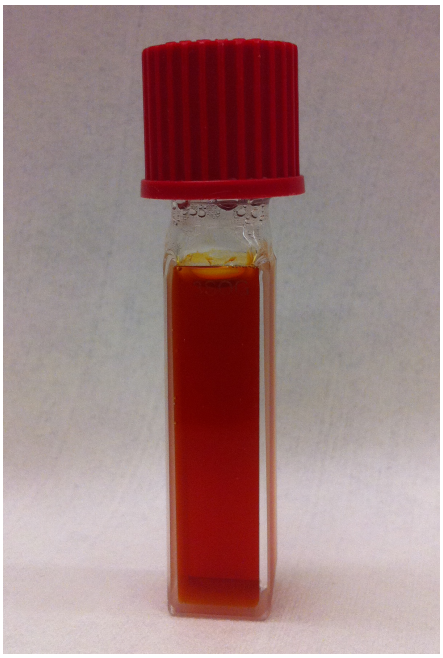

Figure 3.2: Photolytic nanodevice suspension

3.2 Materials Characterization

3.2.1 Ultraviolet/Visible Spectroscopy

Investigations into the optical properties of the nanodevice suspension and its components were carried out through the use of UV-visible spectroscopy. To find the optical transmission spectrum of the photolytic device suspension, a Varian Cary 300 Bio UV-visible spectrophotometer (Agilent Technologies, Wilmington, DE) was employed. This system records the transmission coefficient of a sample within the UV- and visible-light spectrum. Once the optical transmission is recorded, the optical absorbance, A, can be determined by taking the negative logarithm of the transmission coefficient:

$$A = -Log(T) \tag{3.1}$$

For optical absorbance scans of as synthesized and Au NP decorated NWs, photolytic suspensions were diluted 30 times in DI water to ensure an optimized signal to noise, and were

referenced to DI water. To measure the absorption enhancement provided by Au NP decoration, the decorated NWs were referenced to undecorated NWs of the same concentration, both at 30 times dilution. Measurements were taken at 1 nm intervals; with an integration time of 0.1 s. The wavelength range was from 200 nm to 800 nm. To maintain consistency in the data collected, baseline correction was performed, removing any background noise caused by changes in equipment conditions.

3.2.2 Band Gap Estimation of $V_3O_7{\cdot}H_2O$ Nanowires

For determination of the band gap energy (E_g) of $V_3O_7{\cdot}H_2O$, UV-visible spectroscopy was used in the same method as discussed above. For this work, a 0.11 g/L concentration of NWs to DI water was used. After the optical transmission coefficient spectrum was recorded by UV-visible spectroscopy, it was converted to optical absorbance, using the method detailed in Section 3.2.1. The optical absorbance spectrum was then converted from relation to wavelength (nm) to photon energy (eV), and the baseline was removed by subtraction. This subtraction locates the minimum optical absorbance to 0, leaving no offset values for further baseline correction. The logarithm of this optical absorbance spectrum was plotted as a function of photon energy (eV), and a vertical asymptote was observed on the semi-log plot. The value of the photon energy at this vertical asymptotic line was estimated to be the band gap energy (E_g).

3.2.3 Electron Microscopy

For characterization of sol-gel synthesized NWs, Transmission Electron Microscopy (TEM) and Scanning Electron Microscopy (SEM) were conducted at the Oklahoma State University Electron Microscopy Laboratory. For TEM imaging, a JEOL JEM-2100 scanning transmission electron microscope (JEOL Ltd., Tokyo, Japan) was utilized. This experimentation was conducted at an accelerating voltage of 200 kV. For SEM, the FEI Quanta 600 field-emission gun environmental scanning electron microscope (FEI, Hillsboro, Oregon) was used at an

operating voltage of 30 kV. Images from TEM and SEM were used to investigate the size distribution of NWs and NPs, and to verify that the $HAuCl_4$ precursor indeed reduced to Au NPs at the surface of the $V_3O_7{\cdot}H_2O$ NWs. For the determination of the average NW diameter, 20 measurements were obtained from the SEM image. TEM images were used to determine sizes of Au NPs decorating the surface of the NWs using the same procedure.

3.3 Photolysis of Water

3.3.1 Method for Conducting Photolysis

Upon synthesis of the NW-NP conjugate devices suspended in water, a standardized method was required to test their performance as photolytic nanodevices. A rectangular optical cell (Starna Cells, Inc., Atascadero, CA) was first implemented to minimize reflection at the cell walls and increase light absorption efficiency. This cell was held under constant temperature of 40°C, and illuminated for 60 minutes. An Agilent U8001A Single Output DC Power Supply connected to a 5 mm LED RL5-B5515 (λ = 470 nm, viewing angle = 15˚) (SuperBright LEDs, St. Louis, MO) was used as the light source. The power source supplied 3.3 volts (V) and 0.04 amperes (A), producing 8.33 mW. To remove background noise caused by N_2 leakage, a vacuum-sealed method was used.

The final protocol for gas quantification via gas chromatography utilized a crimped aluminum cap to seal the rubber septa, on a cylindrical vial. Initially, a 28 mL balch tube was used to test the vacuum-seal approach, however the significantly higher capacity caused a reduction in production gas concentration. Subsequently a 6 mL autosampler vial (Kimble Chase, Vineland, NJ) was used for gas characterization, due to its reduced headspace volume. This cell was subsequently sealed and vacuumed, to remove excess nitrogen (N_2) and oxygen (O_2) from the cell headspace. After photolysis, gas samples were extracted from the cell and injected into the

GC system via a Hamilton GasTight 1750SL 500 µL syringe (22/2"/5)L (Hamilton Company, Reno, NV). Figure 3.3 shows the photolytic cells used in the present thesis.

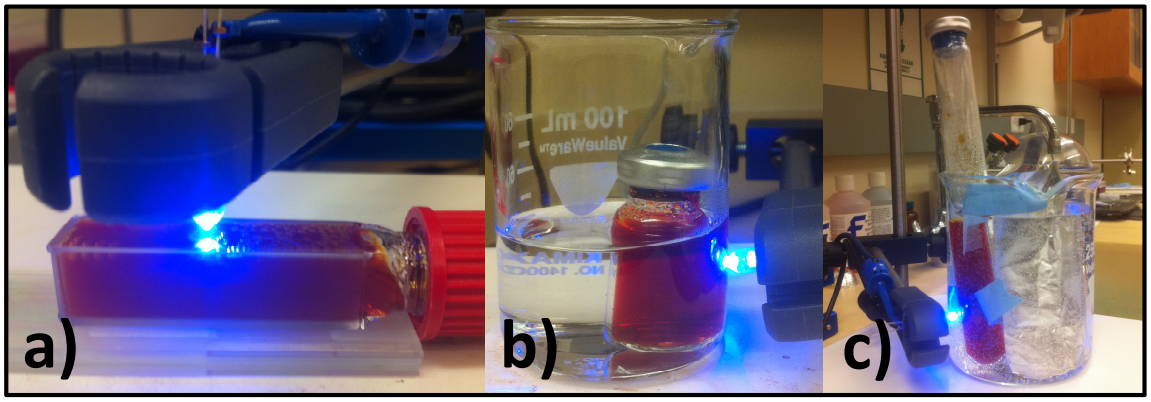

Figure 3.3: Cells used for photolysis: a) vertical illumination into a Starna cell, b) vacuum-sealed autosampler vial, and c) vacuum-sealed balch tube

3.3.2 Characterization and Quantification of Gas Produced

Characterization and quantification of the products of water photolysis was performed through the use of Gas Chromatography (GC), a method by which gas molecules are separated by their volatility, and detected. Each gas interacts with the walls of the GC column in a different manner, and passes through the column at a different rate. For this work, an Agilent 6890N GC (Agilent Technologies, Wilmington, DE) equipped with a Carboxen-1010 PLOT (Porous Layer Open Tubular) capillary column with dimensions of 30 m (length) x 320 µm (inner diameter) x 15 µm (average thickness) (Supelco, Bellefonte, PA) was used. For the method used, the inlet on the GC system was run in "split" mode with a split ratio of 30:1 on injected gases, and the oven temperature was held at 80°C. argon (Ar) was used as the carrier gas with a flow rate of 2 mL/min. For hydrogen (H_2) detection, a thermal conductivity detector (TCD) was used, with the detector temperature held constant at 230°C. This method lasts 7.5 minutes, with the H_2 signal occurring at 1.7 minutes. Chemstation software (Agilent Technologies, Wilmington, DE) was used for analysis and quantification of the concentrations of H_2 in each gas sample injected. After

obtaining a GC spectrum, the gases were identified by their time of elution, and peaks were integrated for comparison with a calibration sample spectrum. Calibration of H_2 was conducted at four levels of known concentrations analyzed from an injection volume of 100 μL. For H_2 calibration, separate mixtures containing 2.5, 3, 3.5, and 4 percent H_2 were used.

For separation of the O_2 peak from N_2, a more complex method was used. This method utilized the same equipment as the method above, however the flow rate was 0.4 mL/min for the first 12 minutes, and increased at a rate of 0.1 mL/min^2 to a final flow rate of 0.8 mL/min until 21 minutes had elapsed. This method used the same split ratio of 30:1 and Ar carrier gas. The initial oven temperature was held at 32 °C for 12 minutes, then increased at a rate of 30 °C/min to a final temperature of 236 °C and held for the final 2.2 minutes. This method lasted a total of 21.2 minutes, with H_2 elution at 8.3 minutes and O_2 elution at 12.1 minutes.

3.3.4 Calculation of Photolytic Efficiencies

The number of moles of H_2 produced was required for the subsequent calculation of photolytic efficiencies. This value was obtained from the GC analysis conducted in Section 3.3.4, in which gas quantification was performed on a percentage basis. To calculate the number of moles of H_2 produced, the peak area was integrated from the GC spectra. The area was compared with a known amount of H_2 from a calibration injection, and the ratio of the areas was taken. For 3% H_2 diluted in Ar in a 100 μL calibration injection, 3 μL of H_2 would be present. The calibration injection was taken at 1 atm, and the volume injected is used to convert the H_2 peak area to a corresponding number of moles (22.4 L/mol at 1 atm). The equation used for this calculation is listed below, where $n_{H_{2exp}}$ is the number of moles of H_2 produced by photolysis, $n_{H_{2cal}}$ is the moles of H_2 in the calibration injection, A_{exp} represents the integrated area of the H_2 peak produced by photolysis, and A_{cal} is the area of the H_2 peak from the calibration injection.

$$n_{H_{2exp}} = n_{H_{2cal}} \times \frac{A_{exp}}{A_{cal}} \tag{3.2}$$

Quantum Efficiency (QE) is the ratio of photons harvested to photons absorbed by the system during photolysis. For the design at hand, the number of harvested photons is found from the moles of H_2 quantified by GC, and calculated above. This term, multiplied by the Avogadro constant gives the moles of H_2 that are produced during this process. The number of photons absorbed is the light energy absorbed by the solution divided by the energy of a single photon. To produce a molecule of H_2, 2 photons are required. Therefore, a multiplication factor of 2 next to the photon energy term is used.

$$Quantum\ Efficiency = \frac{\#\ of\ photons\ harvested}{\#\ of\ photons\ absorbed} \tag{3.3}$$

$$QE = \frac{n_{H_2} \times N_A}{\frac{P \times t \times (1 - R - T)}{2\frac{hc}{\lambda}}} \tag{3.4}$$

Table 3.1: Components of the QE equation for the photolytic nanodevice presented in this thesis

Symbol	Meaning	Value
n_{H_2}	Moles of H_2	moles
N_A	Avogadro's Constant	$6.022 \times 10^{23}\ mol^{-1}$
P	Incident Power	J/s
t	Time of illumination	3600 s
R	Reflection Coefficient	Percent of 100
T	Transmission Coefficient	Percent of 100
h	Planck's Constant	$6.626 \times 10^{-34}\ J/s$
c	Speed of Light	$2.998 \times 10^{8}\ m/s$
λ	Wavelength	$470 \times 10^{-9}\ m$

Internal Conversion Efficiency (ICE) describes the capability of a photolytic device to convert incident photon energy to useable energy (i.e., H_2). The ICE of a photolytic device is calculated by multiplying the QE, obtained above, with the ratio of energy stored in photolytically produced H_2 (1.23 eV), and the photon energy incident on the photolytic cell (2.64 eV) at 470 nm. The specific ICE is a function of the incident photon energy utilized for photolysis. The equation used for the determination of the specific ICE of this device under 470 nm radiation is provided below.

$$Internal\ Conversion\ Efficiency_{\lambda} = QE \times \frac{energy\ stored\ in\ a\ molecule\ of\ H_2}{incident\ photon\ energy} \quad (3.5)$$

$$ICE_{\lambda=470\ nm} = QE \times \frac{1.23\ eV}{2.64\ eV} \quad (3.6)$$

CHAPTER 4

RESULTS AND DISCUSSION

4.1 Scanning Electron Microscopy

To characterize the $V_3O_7{\cdot}H_2O$ NW structures, ensuring they were left intact after the critical drying process, Scanning Electron Microscopy (SEM) was performed with dry aerogel samples. SEM images were also used for measuring the average diameter and length of the $V_3O_7{\cdot}H_2O$ NWs. This work was performed with the help of Ozge Topal and Terry Colberg at the Oklahoma State University Electron Microscopy Laboratory using the method discussed in Section 3.2.3. The aerogel nanostructure used in the present thesis is comprised of a dense collection of NWs, bundled into a "bird's nest" structure as previously described. The average diameter of these NWs was found to be 12.0 nm (± 2.4 nm). Although the aforementioned disordered structure prevented a precise measurement, NWs were found to be greater than 10 μm in length. In Figures 4.2 and 4.3, the high-resolution images of these NW "bird's nest" structures can be seen in detail.

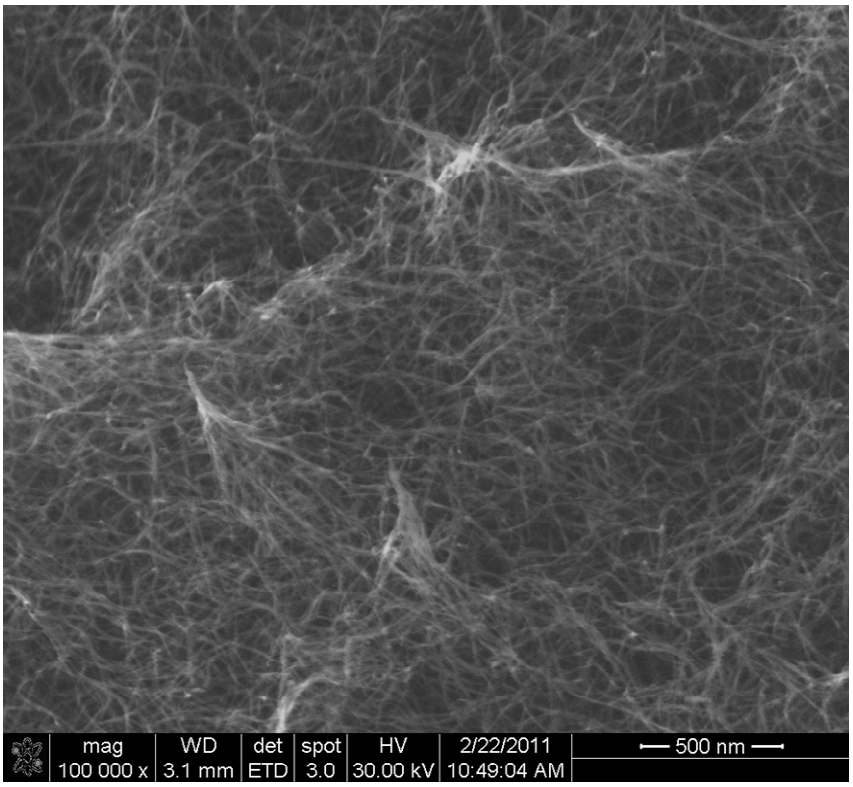

Figure 4.1: SEM image of $V_3O_7 \cdot H_2O$ NWs [O. Topal, T. Colberg]

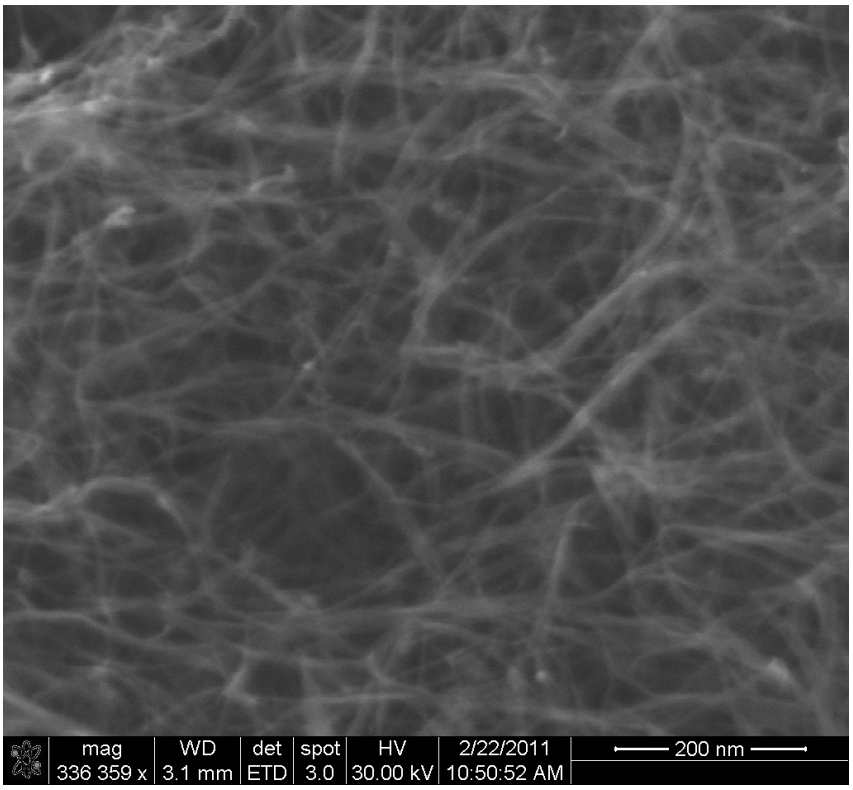

Figure 4.2: SEM image of $V_3O_7 \cdot H_2O$ NWs at increased magnification [O. Topal, T. Colberg]

4.2 Band Gap

The band gap energy (E_g) of $V_3O_7{\cdot}H_2O$ NWs synthesized in this work was estimated to be 2.18 eV, utilizing the method explained in Section 3.2.2. The band gap energy was derived from an optical absorbance spectrum obtained by UV-visible spectroscopy. At the band gap energy, optical absorbance tends towards 0, as there are no electronic transitions in the energy gap. Therefore, when displayed on a plot with the log of optical absorbance as a function of photon energy, the optical absorbance forms an asymptote at the band gap energy. The band gap energy of $V_3O_7{\cdot}H_2O$ was found to be greater than the minimum photon energy of 1.23 eV required for photolytic water splitting, therefore its use as the photoanode is appropriate. In Figure 4.3, the band gap energy of $V_3O_7{\cdot}H_2O$ is estimated as the vertical asymptote, which is indicated by the dotted line.

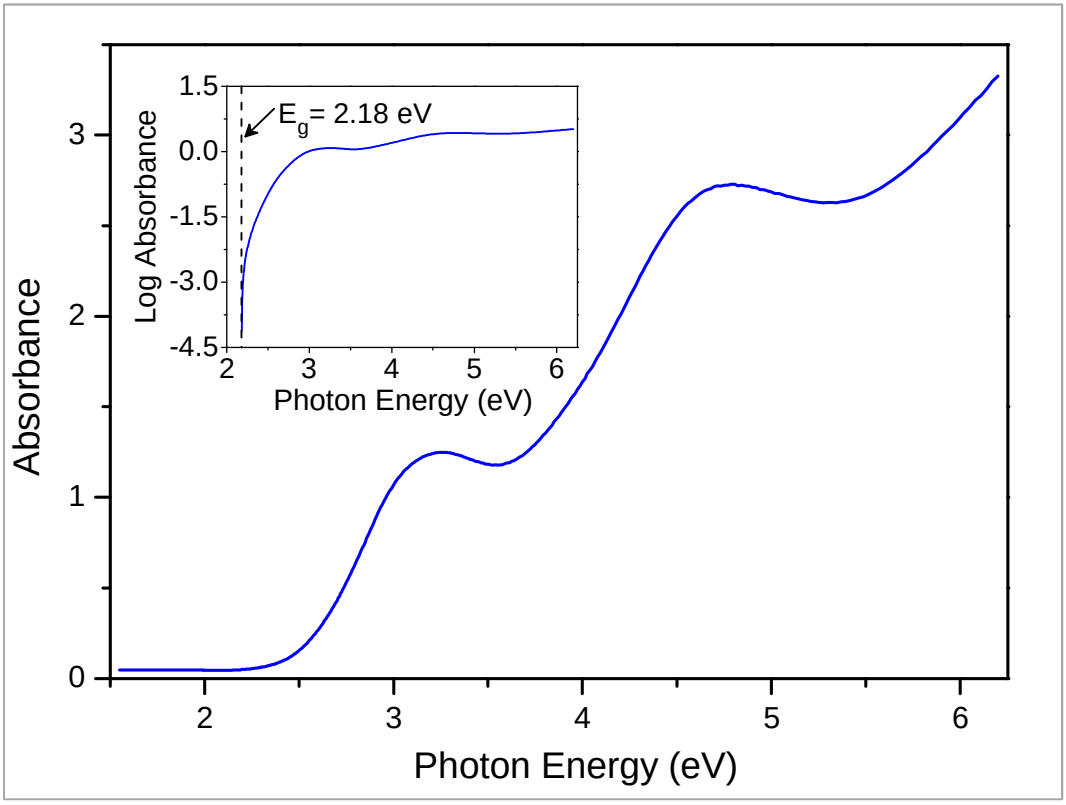

Figure 4.3: Optical absorbance spectrum of $V_3O_7{\cdot}H_2O$ with inlay plot used for band gap estimation

4.3 Transmission Electron Microscopy

Transmission Electron Microscopy (TEM) was used to verify that the precursor chemical, $HAuCl_4$, indeed reduces to Au NPs upon introduction to the $V_3O_7{\cdot}H_2O$ NWs. This method was also used for further characterization of NWs and NPs. TEM was conducted with the help of Ryan Jones and Terry Colberg at the Oklahoma State University Electron Microscopy Laboratory. Figure 4.4 shows $V_3O_7{\cdot}H_2O$ NWs decorated with Au NPs. From TEM imaging, it was shown that Au NPs were produced via the reduction of the $HAuCl_4$ precursor and decorated the surface of $V_3O_7{\cdot}H_2O$ NWs. In Figure 4.4, NW surfaces are seen to be virtually covered with densely packed Au NPs. To further characterize the NW-NP nanodevice suspensions, the average diameter of Au NPs was measured by the TEM image. The average diameter of Au NPs decorating the $V_3O_7{\cdot}H_2O$ NWs was found to be 7.5 nm (± 2.2 nm). For TEM imaging, the concentration of $HAuCl_4$ used was 4 times higher than what was used in the final procedure for NW-NP device fabrication. A lower concentration of $HAuCl_4$ was found to be optimal for gas production, therefore it was implemented for photolysis experiments. The higher concentration of $HAuCl_4$ possibly forms a higher number of Au NPs, densely decorating the surface of the NWs. Advantages of higher Au NP concentration include increased scattering and a larger cathodic area (i.e.: lower polarization at the cathode). However, as a consequence of higher Au NP concentration, the surface area of NWs for the anodic reaction (i.e.: larger anodic polarization) is reduced.

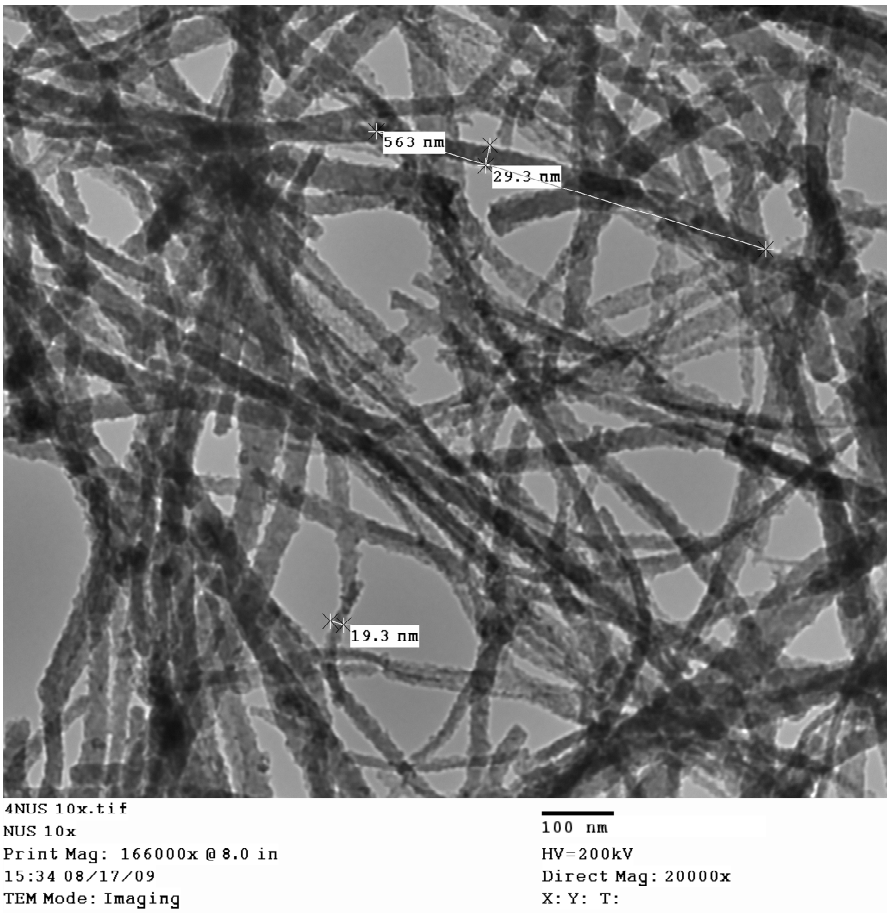

Figure 4.4: TEM image of $V_3O_7{\cdot}H_2O$ NWs decorated by Au NPs [R. Jones, T. Colberg]

4.4 Optical Absorption

Suspensions of decorated and undecorated NWs were characterized using the optical absorption method discussed in Section 3.2.1. The optical enhancement due to Au NP decoration of NWs can be seen in Figure 4.5, which displays the optical absorbance spectra of identically concentrated suspensions of NWs; one solution decorated with Au NPs and the other undecorated. The optical absorbance spectrum of decorated NWs shows similar peaks at 263 and 378 nm as undecorated $V_3O_7{\cdot}H_2O$, as well as the formation of new peaks at 217 nm and 408 nm. The 217 nm peak in literature is attributed to excess $HAuCl_4$ in the suspension, the precursor chemical for Au NPs. However, as a consequence of Au NP decoration, the peak at 408 nm may

be attributed to NW waveguide modes enabled by NW-NP conjugation. It is known from literature that Au NPs display a distinct absorbance peak at 525 nm, therefore these newly formed peaks would not be attributed to the Au NPs alone. In addition, an overall enhancement of optical absorbance is viewed from 200 to 600 nm. It is possible this effect can be attributed to the formation of V_2O_5, a vanadium oxide at its highest oxidation state (+5). Since $V_3O_7{\cdot}H_2O$ exhibits a mixed oxidation state (+4 and +5), it is possible that a surface transformation to V_2O_5 may occur with the introduction of Au NPs, further oxidizing the NW surface, which may explain the addition of new peaks.

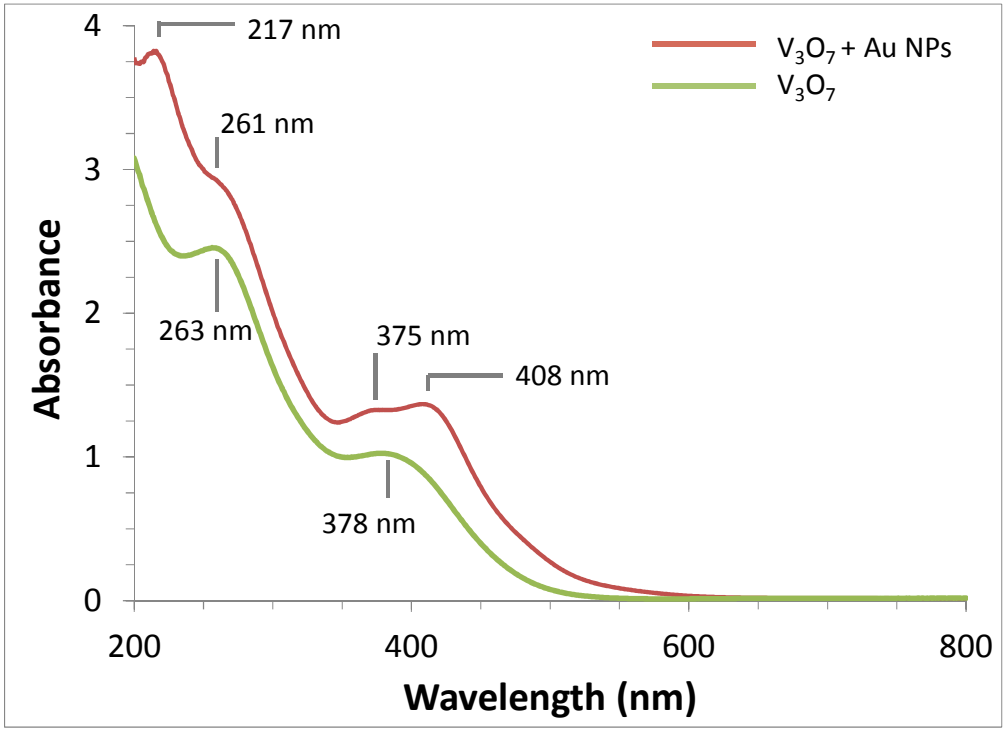

Figure 4.5: Optical absorbance spectra of decorated and undecorated $V_3O_7{\cdot}H_2O$ NWs

Figure 4.6 illustrates the difference in optical absorbance of decorated NWs to undecorated NWs, and the wavelength positions of the newly created peaks are shown. When comparing optical absorbance spectrum of Au NP-decorated NWs to that of undecorated NWs, a distinct peak at 222 nm is seen that can be attributed to excess $HAuCl_4$ in the suspension [22]. However, the presence of optical absorbance peaks at 285, 423, and 483 nm may also result from

coupling of light to waveguide modes of the $V_3O_7{\cdot}H_2O$ NWs. When referencing the decorated NWs to undecorated V_2O_5 NWs, the same peaks appear, eliminating the possibility that the new peaks are attributed only to surface transformation of the NWs. Previous investigations regarding NW waveguide modes have shown that the presence of scatterers (i.e., plasmonic metal NPs) on the surface of a waveguide can enhance the coupling of incident radiation to the waveguide modes. In the work by Stuart and Hall, this optical absorption enhancement effect was demonstrated with Ag NPs on semiconductor thin films [21]. The Au NPs can futher enhance the optical absorption in $V_3O_7{\cdot}H_2O$ NWs due to a different mechanism. In the TEM image of Figure 4.4, Au NPs (average diameter 7.5 nm) were observed to densely decorate the surface of the NWs. For the NW-NP conjugate concept, Au NPs acting as near-field concentrators can enhance optical absorption due to their proximity to the semiconductor NW waveguides. Combined with possible near-field enhancement effects from surrounding NPs, the NW-NP conjugate concept presents an ideal platform for optical enhancement via plasmonic effects of the metal NPs.

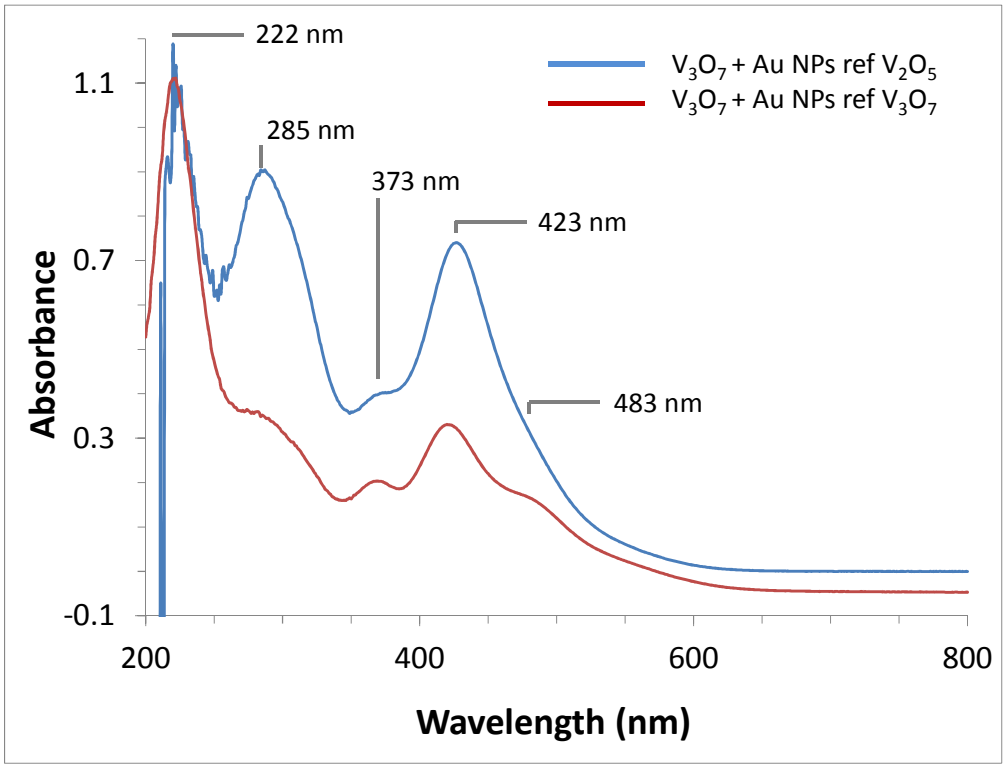

Figure 4.6: Optical absorbance spectrum of Au NP-decorated NWs referenced to undecorated NWs

4.5 Photolysis of Water

Photolytic splitting of water was conducted using the methods described in Section 3.3.1. When irradiating the photolytic nanodevice suspension with visible light (λ = 470 nm) at an incident power of 8.33 mW, photolytic gas production was observable to the naked eye. Figure 4.7 shows the nanodevice suspension after photolysis was conducted for 60 minutes. Production of gas bubbles was observed to be consistent for 60 minutes, after which it diminished. This could be due to adsorption of photolysis products to the NW or NP surfaces, reducing the effective surface area for redox reactions (charge transfer). The rapid production of gases was not observed when irradiating undecorated NW suspensions, making the conjugation of $V_3O_7{\cdot}H_2O$ NWs with Au NPs a necessary condition for photolysis. Since photolysis was not observed in the absence of the NPs, the role of Au NPs as the cathode is confirmed.

Figure 4.7: Gas bubbles generated after photolysis

4.6 Gas Chromatography

Utilizing Gas Chromatography (GC), the gases produced during photolysis were analyzed for identification and quantification. The GC spectra obtained after photolysis are shown in Figures 4.8 and 4.9, where H_2 appears at 1.7 minutes in the GC spectra shown, and O_2/H_2 coelute to form one large peak at 2.1 minutes. Gas spectra obtained from photolysis gas samples are compared with a spectrum from ambient air in Figure 4.9. When comparing the nitrogen (N_2) signal from an injection of ambient air to the vacuum-sealed photolysis injection, the signal from the vacuumed vial is an order of magnitude reduced, but continues to dominate the spectrum on a percentage basis. This leakage is a common artifact with GC conducted in air environment; therefore it does not signify the production of N_2. The production of H_2 was consistent for subsequent demonstrations of photolysis, and was repeatable for multiple nanodevice suspensions synthesized over several months. After photolysis, multiple injections from the same gas sample were taken to ensure the signals were not artifacts caused by outside conditions. Subsequent samples from gas produced by photolysis of water show a significant increase in the N_2 signal as well as a reduction in the signals from photolysis products. The N_2 signal increase is explained by the large percentage of N_2 (78%) in the air surrounding the GC, and is common with low concentrations of gases from a sample. Since this process was performed under near-vacuum conditions, the infiltration of air after multiple injections is inevitable. As produced gases are extracted from the sampling vial, the signal areas are diminished and N_2 and O_2 are noticeably increased. The correlated reduction of peaks not associated with ambient air (i.e., H_2, CO_2, H_2O vapor) illustrates this point.

The secondary GC protocol was employed for resolution of O_2 separate from the N_2 peak. Figures 4.10 and 4.11 display the GC spectra obtained by the use of this method and its comparison with an identical volume injection of ambient air. The secondary GC method separates the O_2 from the N_2 peak accurately, giving an undistorted signal. H_2 elutes at 8.3

minutes for this method and O_2 is seen at 12.1 minutes. The baseline increase beginning at 12 minutes is due to the ramp in carrier gas flow rate as well as an oven temperature ramp. Figure 4.10 shows the GC spectrum of an injection of ambient air, with an inset of the O_2 and N_2 split peaks. In Figure 4.11, the GC spectrum from photolysis products is shown, with a significant H_2 peak as well as the split peaks of O_2 and N_2. This method allowed an investigation into O_2 production, as well as the further validation of H_2 production given by the initial GC method. Consistent H_2 production was observed as a result of this study, and a recordable amount of O_2 produced. For O_2 investigation, the gas sample was retrieved from within a N_2 and H_2 glovebox. Since ambient air contains 21% O_2, any leakage from the ambient environment can cause significant increases in the O_2 signal. H_2 production was not recorded for this work, since the glovebox ambient contained up to 1% H_2.

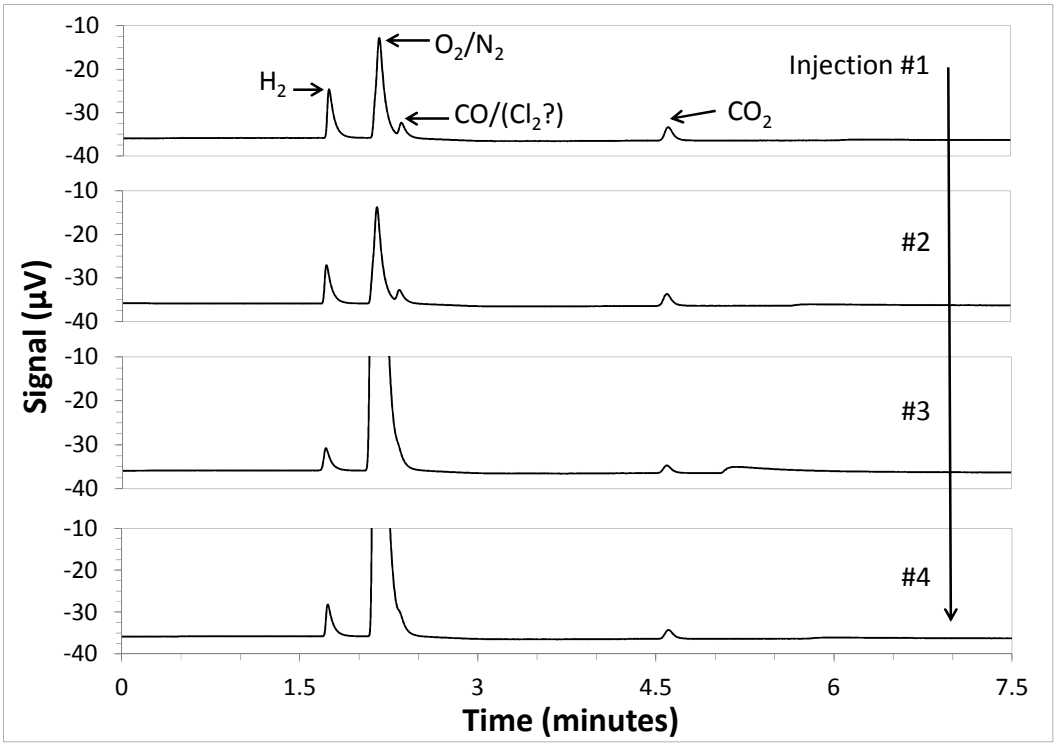

Figure 4.8: GC spectra showing H_2 production from photolysis

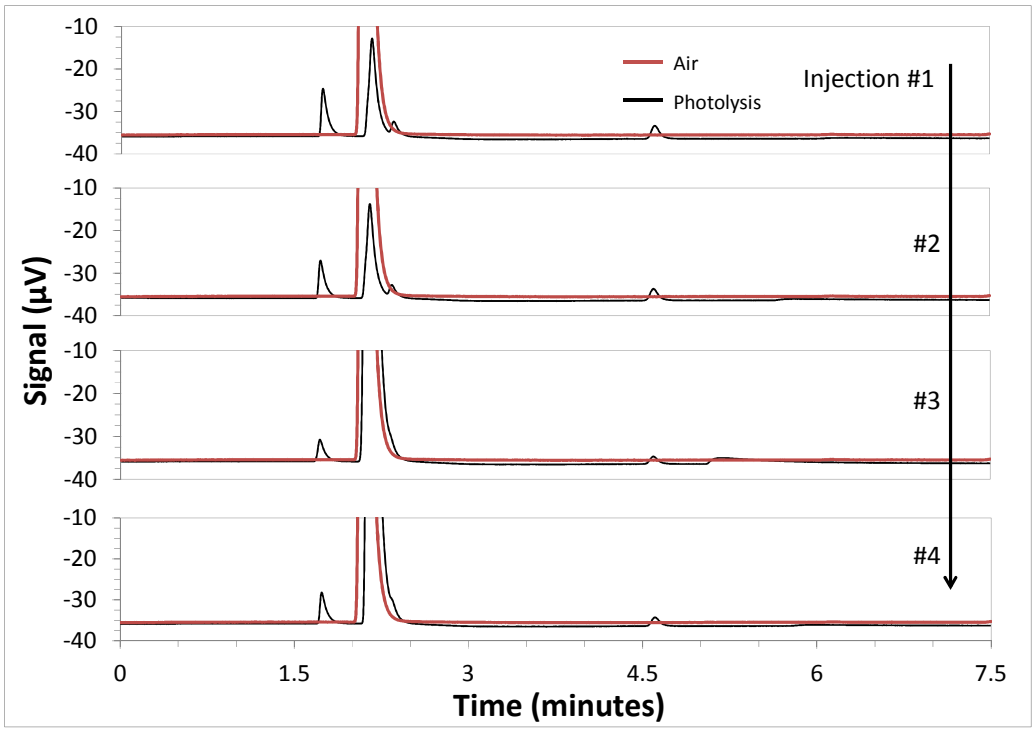

Figure 4.9: GC spectra comparing photolysis products to ambient air

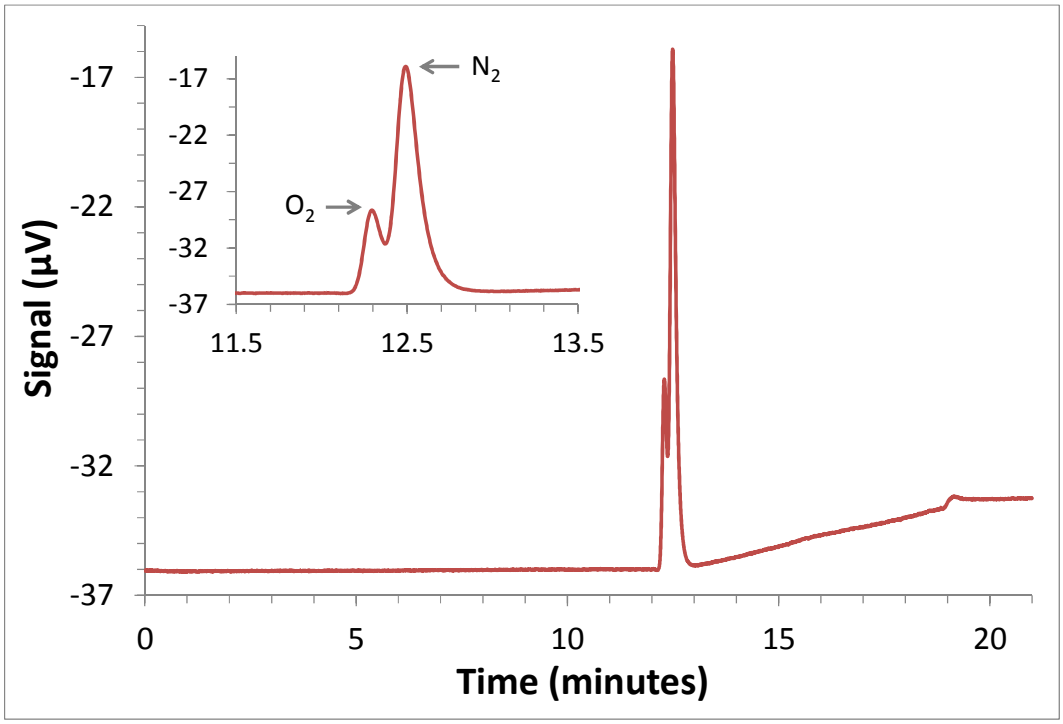

Figure 4.10: GC spectrum showing separation of O_2 and N_2 peaks in air using secondary method

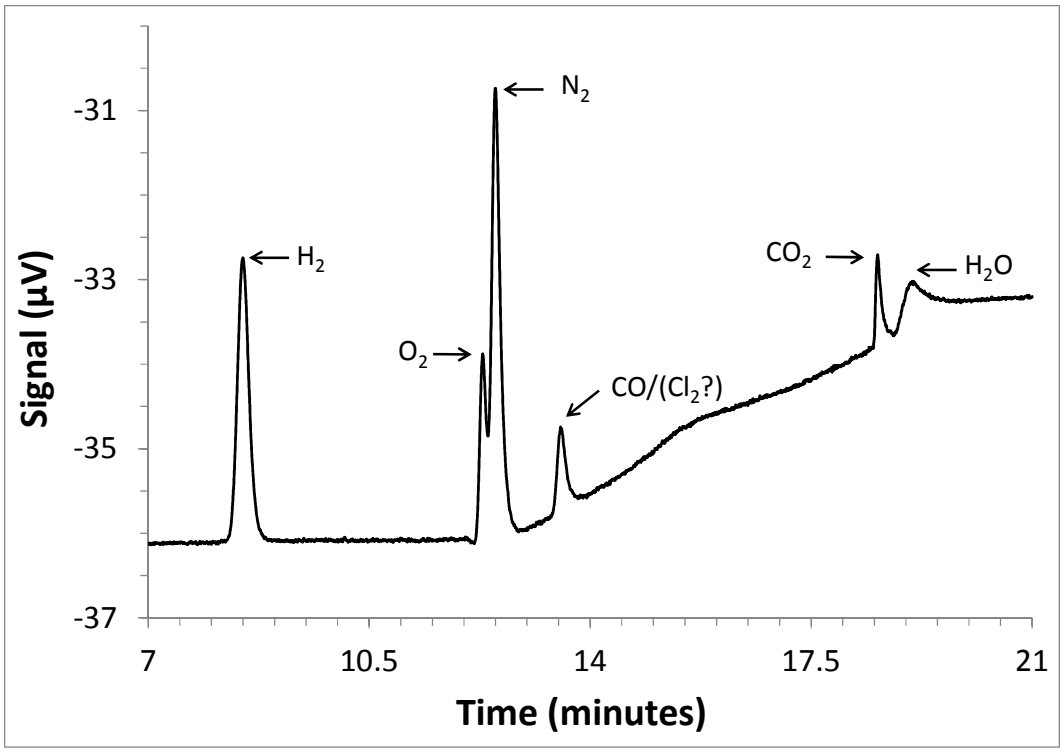

Figure 4.11: GC spectrum of photolysis products using secondary method

4.7 Quantum and Internal Conversion Efficiency

Using the results from GC, photolytic efficiencies were recorded using the methods discussed in the previous chapter. The Quantum Efficiency (QE) and Internal Conversion Efficiency (ICE) of the concept developed in this thesis were calculated using the following equations:

$$QE = \frac{n_{H_2} \times N_A}{\frac{P \times t \times (1 - R - T)}{2\frac{hc}{\lambda}}} \tag{4.1}$$

$$ICE_{\lambda=470\,nm} = QE \times \frac{1.23\,eV}{2.64\,eV} \tag{4.2}$$

After 60 minutes of photolysis, the highest amount of H_2 produced was found to be 567.7×10^{-8} moles. This quantity was used in conjunction with the equations listed above, resulting

in a QE and ICE of 19.28% and 8.98%, respectively. The nanodevice conjugate concept presented in this thesis marks a significant step forward in visible-light driven devices, as the previous benchmark value for QE for such visible-light devices has been widely regarded to be 10% [13].

In addition to the quantification of H_2, the secondary GC protocol was used for verification of O_2 production and analysis of stoichiometry. Using this GC method, it was determined that significant O_2 was produced during this process. However, the ratio of H_2 to O_2 moles was found to be 4.75:1, more than double the expected ratio of 2:1 H_2 to O_2. This could be attributed to any number of factors; however the accuracy and reproducibility of the O_2 quantification must be assured first.

CHAPTER 5

CONCLUSIONS

This chapter presents the conclusions drawn from the results of the present thesis. Suggestions for further work are also provided.

1. A novel device architecture for photolytic production of H_2 from water was proposed and investigated. This architecture consists of semiconductor nanowires decorated with metal nanoparticles. The proof of the concept was accomplished using sol-gel synthesized $V_3O_7{\cdot}H_2O$ nanowires decorated with Au nanoparticles, which were synthesized by chemical reduction. The nanowire-nanoparticle conjugate devices are obtained in the form of a suspension in water. Analysis of the photolytic product by gas chromatography confirmed production of H_2 and O_2 under 470 nm radiation.
2. In particular a Quantum Efficiency (QE) of 19.28% and Internal Conversion Efficiency (ICE) of 8.98% were demonstrated for the first hour of photolysis when 470 nm LED irradiation was used. The author considers this result a significant achievement. Photolytic devices reported in the literature so far could not perform more than few percent of ICE. Further, photolysis was limited to only higher energy edge of the visible range (i.e., $\leq$ 420 nm). In addition, the QE value demonstrated in this thesis is competitive with many designs that have been demonstrated using visible light and surpasses the previously theorized limit of 10% QE.

3. The band gap energy of $V_3O_7 \cdot H_2O$, an essentially undiscovered semiconductor, is estimated at 2.18 eV through the use of UV-visible spectroscopy. This band gap meets the minimum necessary requirement for photolysis of water which is 1.23 eV. Further, it is significantly lower than the band gaps of transition metal oxides (TMO) for which photolysis was demonstrated in the past. The substantial benefit of this lower band gap is higher optical absorption in the visible spectrum. A measureable enhancement in optical absorption is discovered for $V_3O_7 \cdot H_2O$ NWs when they are decorated with Au NPs. This enhancement is also accompanied with the formation of new peaks in the optical absorption spectrum. These new peaks are attributed to coupling of incident light to waveguide modes in $V_3O_7 \cdot H_2O$ NWs. Here, Au NPs serve as the light couplers through scattering. Bending of light in the direction of the NW axis increases the optical absorption. A further enhancement mechanism is the near-field concentration of incident light at the proximity of NPs due to localized surface plasmon resonance.
4. A significant degradation in photolysis is found after two hours of operation under the conditions mentioned in this thesis. However, keeping the NW-NP suspension in dark overnight regenerates the photolytic devices to a large degree (i.e., >75%). This quasi-degradation effect is attributed to weak bonding of photolytic products (e.g., H, O, O_2) to the $V_3O_7 \cdot H_2O$ and Au surfaces.
5. Future work must study the kinetics of gas production with direct connection to GC for real-time analysis. The kinetics of gas production can elucidate the mechanism of degradation.
6. Dependence of the QE on nanowire diameter should be studied. The efficiency is expected to drop with increasing diameter due to the longer distance that electrons and holes have to travel before they are channeled to the redox reactions. With longer distance, the probability of electron-hole recombination is higher. In addition, the hypothesis of coupling of light into NW waveguide modes should be tested also by

varying the NW diameter. As a first order estimate, the coupling should increase with increasing NW diameter.

7. The present thesis already demonstrated gas bubbling at lower photon energies (higher wavelengths), i.e., 2.36, 2.05, 1.98 eV (525, 605, and 625 nm, respectively). However, neither the gas was analyzed nor efficiency was evaluated. The future work should carry out gas analysis and efficiency determination for these photon energies. Analysis of photolysis under direct sunlight would also be a valuable investigation for real-world application, as well as being a large milestone for scalable device demonstration.
8. It is theorized that Au NPs mediate the coupling of incident light into NW waveguide modes. This hypothesis should be tested by finite time domain simulations. Also, a necessary condition for this effect is a high refractive index contrast between water and $V_3O_7{\cdot}H_2O$. Hence, the refractive index of $V_3O_7{\cdot}H_2O$ must be derived experimentally. A valid technique would be the simple refraction experiment for the NW suspension and use of the effective medium theory.
9. UV-photoelectron spectroscopy (UPS) should be utilized to investigate the valence band edge energy level of $V_3O_7{\cdot}H_2O$. With this information, combined with the band gap energy calculated in the present work, both conduction and valence band edge energy levels can be determined to further explain/verify the mechanism of photolysis.

REFERENCES

[1] U.S. Dept. of Energy. (2010). "World Energy Outlook 2010." Retrieved February 12, 2011, from http://www.eia.doe.gov/oiaf/ieo/world.html.

[2] U.S. Dept. of Energy. (Dec 2001). Energy Efficiency and Renewable Energy Technology Validation, Hydrogen Properties, *Hydrogen Fuel Cell Engines and Related Technologies*.

[3] Fujishima, A. and K. Honda (1972). "Electrochemical Photolysis of Water at a Semiconductor Electrode." Nature **238**(5358): 37-38.

[4] Ç. Ö. Topal, "Light-Induced Transformation of Nanostructured $V_3O_7{\cdot}H_2O$ to V_2O_5," Master's Thesis, Oklahoma State University, (2010).

[5] Sander, M. U., K. Luther, et al. (1993). "On the Photoionization Mechanism of Liquid Water." Berichte der Bunsengesellschaft für physikalische Chemie **97**(8): 953-960.

[6] Sayama, K., Arakawa, et al. (1996). "Photocatalytic water splitting on nickel intercalated $A_4Ta_xNb_{6-x}O_{17}$ (A = K, Rb)," Catalysis Today, **28**(1-2), 175-182.

[7] Kawai, T. and T. Sakata (1979). "Hydrogen evolution from water using solid carbon and light energy." Nature **282**(5736): 283-284.

[8] Borgarello, E., J. Kiwi, et al. (1981). "Sustained water cleavage by visible light." Journal of the American Chemical Society **103**(21): 6324-6329.

[9] Varghese, O. K., M. Paulose, et al. (2005). "Water-Photolysis Properties of Micron-Length Highly-Ordered Titania Nanotube-Arrays." Journal of Nanoscience and Nanotechnology **5**(7).

[10] Zou, Z., J. Ye, et al. (2001). "Direct splitting of water under visible light irradiation with an oxide semiconductor photocatalyst." Nature **414**(6864): 625-627.

[11] T. E. Mallouk, "The emerging technology of solar fuels," J. Phys. Chem. Lett. 1, 2110-2111 (2010).

[12] Grätzel, M. (2001). "Photoelectrochemical cells." Nature **414**(6861): 338-344.

[13] Osterloh, F. E. (2007). "Inorganic Materials as Catalysts for Photochemical Splitting of Water." Chemistry of Materials **20**(1): 35-54.

[14] Nam, Y. S., A. P. Magyar, et al. (2010). "Biologically templated photocatalytic nanostructures for sustained light-driven water oxidation." Nat Nano **5**(5): 340-344.

[15] Leventis, N., C. Sotiriou-Leventis, et al. (2008). "Polymer nanoencapsulated mesoporous vanadia with unusual ductility at cryogenic temperatures." Journal of Materials Chemistry **18**(21): 2475-2482.

[16] Kato, H., K. Asakura, et al. (2003). "Highly Efficient Water Splitting into H2 and O2 over Lanthanum-Doped NaTaO3 Photocatalysts with High Crystallinity and Surface Nanostructure." Journal of the American Chemical Society **125**(10): 3082-3089.

[17] Maeda, K., K. Teramura, et al. (2006). "Photocatalyst releasing hydrogen from water." Nature **440**(7082): 295-295

[18] Smith, W., S. Mao, et al. (2010). "The effect of Ag nanoparticle loading on the photocatalytic activity of TiO2 nanorod arrays." Chemical Physics Letters **485**(1-3): 171-175.

[19] Sá, J., M. Fernández-García, et al. (2008). "Photoformed electron transfer from TiO2 to metal clusters." Catalysis Communications **9**(10): 1991-1995.

[20] Imamova, S., N. Nedyalkov, et al. (2010). "Near field properties of nanoparticle arrays fabricated by laser annealing of thin Au and Ag films." Applied Surface Science **257**(3): 1075-1079.

[21] Stuart, H. R. and D. G. Hall (1998). "Enhanced Dipole-Dipole Interaction between Elementary Radiators Near a Surface." Physical Review Letters **80**(25): 5663.

[22] Li, X.-z., Q.-f. Lu, et al. (2010). "Template- and micelle-free synthesis of rod-like gold nanoparticles with UVA irradiation." Optoelectronics Letters

VITA

Sean Kelly Maclaskey

Candidate for the Degree of

Master of Science

Thesis: NANOWIRE-NANOPARTICLE CONJUGATE PHOTOLYTIC DEVICES FOR RENEWABLE HYDROGEN PRODUCTION

Major Field: Mechanical and Aerospace Engineering

Biographical:

Personal:

Born on March 5, 1987 in Wichita, Kansas.

Education:

Completed Bachelor of Science in Aerospace Engineering at Oklahoma State University, Stillwater, Oklahoma in May, 2009.

Completed the requirements for the Master of Science in Mechanical and Aerospace Engineering at Oklahoma State University, Stillwater, Oklahoma in June, 2011.

Experience:

Worked as Design Engineer Intern at Cessna Aircraft Company in Wichita, Kansas

Worked as Teaching Assistant in Mechanical and Aerospace Engineering at Oklahoma State University in Stillwater, Oklahoma

Worked as Research Assistant in the Functional Nanomaterials Laboratory at Oklahoma State University in Stillwater, Oklahoma

Professional Memberships:

Student Member of American Institute of Aeronautics and Astronautics

Certifications:

FAA Private Pilot Certification

Engineer in Training (EIT) Certification

Name: Sean Kelly Maclaskey Date of Degree: July, 2011

Institution: Oklahoma State University Location: Stillwater, Oklahoma

Title of Study: NANOWIRE-NANOPARTICLE CONJUGATE PHOTOLYTIC DEVICES FOR RENEWABLE HYDROGEN PRODUCTION

Pages in Study: 42 Candidate for the Degree of Master of Science

Major Field: Mechanical and Aerospace Engineering

Scope and Method of Study:
A clean energy driven economy requires renewable production of zero-emission fuels, such as hydrogen (H_2). Photocatalytic generation of H_2 is one such method to fulfill this demand. Photocatalytic water splitting is an electrochemical process driven by solar energy to produce H_2. Although there have been many investigations on photocatalytic water splitting, the number of concepts utilizing visible light is limited. In the present study, H_2 evolution from water splitting is demonstrated using the novel concept of nanowire-nanoparticle (NW-NP) conjugate devices irradiated by visible light. Photolytic nanodevice suspensions are fabricated via sol-gel synthesis of vanadium oxyhydrate ($V_3O_7{\cdot}H_2O$) NWs, followed by solution chemistry with $HAuCl_4$ for reduction of gold (Au) NPs on the NW surfaces. Characterization of nanodevices was performed via TEM, SEM, and optical spectroscopy. Products of photolysis were quantified and analyzed by Gas Chromatography (GC). The performance of the nanowire-nanoparticle conjugate devices was compared with previous photolytic device designs by the use of quantum and internal conversion efficiencies (QE and ICE, respectively).

Findings and Conclusions:
The present thesis demonstrates photocatalytic production of H_2 using $V_3O_7{\cdot}H_2O$ NW - Au NP conjugate devices under 470 nm excitation. The "photolytic nanodevice suspension in water" concept poses the potential for scalable H_2 production, in addition to the provision for a low-cost technique due to fabrication by sol-gel synthesis and solution chemistry. The $V_3O_7{\cdot}H_2O$ aerogel, a recently discovered semiconductor material, is found to be a suitable photoanode due to its narrow band gap energy of 2.18 eV, and its stability during photolysis. The diameters of the $V_3O_7{\cdot}H_2O$ NWs are found to be 12 nm (± 2.4 nm) from SEM images. The decoration of NWs with Au NPs is verified by TEM imaging and Au NPs are estimated to be 7.5 nm (± 2.2 nm) in size. After decoration of NWs by Au NPs, a near-field enhancement effect on optical absorption by NWs was observed by UV-visible spectroscopy. Further, the emergence of new optical absorbance peaks indicates possible coupling of incident light into waveguide modes of the NWs. QE and ICE values for the NW-NP conjugate devices are found to be 19.28% and 8.98%, respectively, for the first hour of photolysis.

ADVISER'S APPROVAL: Dr. A. Kaan Kalkan